Journal of Industrial Information Integration 41 (2024) 100660

Contents lists available at ScienceDirect

Journal of Industrial Information Integration

journal homepage: www.sciencedirect.com/journal/journal-of-industrial-information-integration

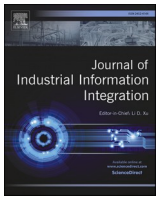

A Cost-effective approach for quality control in PLA-based material extrusion 3D printing using 3D scanning

Andrea Montalti *, Patrich Ferretti, Gian Maria Santi

Department of Industrial Engineering, Alma Mater Studiorum University of Bologna, Viale del Risorgimento 2, 40136 Bologna BO, Italy

ARTICLE INFO

Keywords:
Material extrusion
3D scanning
Quality control
Dimensional accuracy
Cost-effective

ABSTRACT

In this article, our aim is to underscore the importance of verifying that components produced through material extrusion additive manufacturing exhibit geometric and dimensional conformity with the STL (Standard Tessellation Language) model. Currently, the business world is heavily investing in additive technologies, but it is crucial to obtain feedback on the accuracy of the printed component without excessive economic expenditure. For this reason, we have opted to utilize a mid-range 3D scanner (Revopoint Mini with an accuracy of 0.02 mm) to investigate any disparities in print results using PLA material. Each model has been scanned and compared with the initial mesh to qualitatively and quantitatively assess the present errors. The analysis has revealed that the majority of features can be effectively controlled, while the remaining ones either fall within the tool's precision or necessitate a higher-quality scan. Particularly in the analysed case, flat surfaces, profiles of complex geometries, and holes have demonstrated dimensional and geometric controllability. However, details of reduced dimensions or those difficult to reach by the scanner do not allow for adequate comparison due to excessive standard deviation in the error. The analysed layer heights do not exhibit a significant impact on component accuracy.

1. Introduction

3D printing [1] enables rapid realization of prototypes [2] and functional components, transforming a digital model into a tangible reality. Additive manufacturing processes vary, each possessing unique characteristics, yet all share a commonality: layer-by-layer generation of the piece. The technology that birthed additive manufacturing is material extrusion (MEX) [3], where material deposition occurs through a calibrated nozzle, forming each layer; repeating this process at increasing heights enables piece generation along parallel planes.

Currently, this technology enables printing with various materials, among which the most common is PLA (Polylactic Acid) [4,5]. PLA is highly favoured for its ease of printing and the wide range of available colours, which have contributed to its extensive use, particularly in hobbyist applications and for creating initial versions of functional prototypes. Furthermore, its low cost, biodegradability, and the abundance of research on this material have established it as the most widely utilized printing material globally.

For applications requiring superior properties, materials such as PETG [6], ABS [7], TPU [8], and NYLON are available, each offering various colour options and the possibility of incorporating different additives [9]. For advanced requirements, materials enhanced with additives or fibres [10] can be employed, though these often necessitate specialized machinery [11]. Beyond the variety of materials, the architectures of the machines themselves have evolved to enhance print quality and process efficiency [12]. This has led to the development of machines with enclosed and heated chambers, multi-extruder/multi-material [13] systems, and advanced calibration mechanisms.

These advancements underscore the significant progress in the field of 3D printing, allowing for more sophisticated and higher-quality outputs while accommodating a broader range of material properties and application requirements. Component realization begins with a 3D CAD model [14], converted into a mesh and processed within a slicer. Output from the software comprises instructions guiding the machine in piece creation. Currently, most fused deposition printers lack feedback control regarding their spatial positioning, potentially resulting in dimensional and geometric errors imperceptible to the naked eye.

Companies are increasingly employing these technologies [15] for small batch production rather than solely rapid prototyping,

* Corresponding author.
E-mail address: andrea.montalti8@unibo.it (A. Montalti).

https://doi.org/10.1016/j.jii.2024.100660

Available online 4 July 2024

necessitating correct dimensional realization of components. Evaluating dimensional correctness requires the right tool for quality control without significant economic outlay. In certain sectors like aerospace [16] and motorsport [17], there are no significant budget constraints concerning quality control [18]. However, in other sectors, budget considerations weigh heavily. Traditional measuring instruments are typically used but are inadequate for complex surface profiles, necessitating a suitable and flexible tool for any component.

In the academic literature, there are studies that investigate dimensional accuracy, surface roughness [19], and the internal voids within printed components using sophisticated equipment [20] such as Computed Tomography (CT) and Scanning Electron Microscopy (SEM). These tools facilitate the acquisition of highly precise images of both the internal and external geometries of components. The operation and interpretation of these imaging technologies require a high level of expertise, rendering them suitable for medium to high-level components. It is impractical to employ these tools for analysing small batches or lower-tier components, as the costs associated with the equipment and the specialised personnel required for these measurements are not economically justifiable.

Another method for verifying the dimensional accuracy of 3D printed components involves the use of optical and 3D scanning systems [18]. These systems capture a point cloud to virtually replicate the component's geometry, which can then be compared to the original CAD model. There are already companies and academic papers that utilise these technologies for dimensional checks on printed components [21–23]. However, the economic challenge remains significant because such equipment entails substantial costs, which are typically amortised over several years of frequent use. Consequently, there is a growing need to validate the effectiveness of more affordable tools that can still assist in the geometric and dimensional verification of components.

Several types of 3D scanning systems exist, including structured light laser scanners [24], time-of-flight (TOF) lasers [25], blue light scanners, photogrammetry [26], and ultrasound [27]. Excluding ultrasound, which requires high-level hardware, and photogrammetry, which is suitable primarily for large-scale components (measured in metres), the remaining systems—utilising lasers, cameras, and sensors—are relatively cost-effective. Among these, blue light systems are particularly noteworthy for their affordability and effectiveness. These systems employ stereo cameras to capture the shape of the object and generate a point cloud [28]. The precision of the scanning process is also influenced by the management software within the scanner and the post-processing of the point cloud data.

In this paper, we focus on various profiles to evaluate the dimensional and shape accuracy of components produced through Material Extrusion (MEX). Our emphasis is on exploring the use of an economically accessible 3D scanning system for this purpose.

In this article, we focus on evaluating the dimensional and shape accuracy of components produced through Material Extrusion (MEX) using a cost-effective 3D scanning system. Our aim is not to explore the relationship between geometric and dimensional parameters and the printing parameters [30,31], as this has already been extensively examined in the literature [32,33]. Instead, we aim to provide insights into the practical application and efficacy of an accessible scanning system in assessing the quality of 3D printed components.

2. Materials and methods

The workflow depicted in Fig. 1 outlines the steps to be followed in comparing the virtual model with the scanned model. Initially, it is necessary to identify the geometry for analysis, taking care to avoid selecting components with deep cavities or areas inaccessible to the scanner. The second step involves fabricating the component using MEX technology, creating multiple specimens from the same input information (G-code) to highlight the machine's accuracy and repeatability. The third step entails scanning all components with maximum precision. Finally, the last two steps involve the comparison and analysis between the reference model and the scans (Fig. 2).

In this study, the Revopoint Mini [34] was chosen due to its classification as a low-cost scanner [35], making it easily implementable in the industrial realm for geometry verification [36,37] and reverse engineering [38] of components that do not warrant higher-cost equipment purchases. The analysis focused on a specific component encompassing various features common to most components, but the methodology can be replicated for any geometry.

The chosen component for analysis is a gas cam for a motocross bike. The component has been modified from the production piece to adapt the motorcycle to the rider's characteristics, specifically by reducing the throttle opening angle.

This geometry was selected because it encompasses a diverse range of features typically found in 3D printed components, such as a large outer diameter, a small-diameter hole, a flat surface, a complex profile, and an overhanging section. These characteristics are crucial as they enable a comprehensive analysis of features that are more or less susceptible to errors. The inclusion of such varied elements ensures that the evaluation covers a broad spectrum of potential issues and provides a robust basis for assessing the accuracy of 3D printed objects.

The CAD model has been converted into an STL file with a high mesh finishing degree so as to exclude any approximation errors caused by mesh generation. The tessellation has been set with a chord deviation of 0,003 mm and an angle deviation of 0,5°. Each specimen was printed using three different layer heights: 0.1 mm, 0.15 mm, and 0.2 mm. For each layer height, a G-code was generated for a single component and printed three times. Producing three components from the same G-code file allows for the creation of a more robust sample set, taking into account the repeatability errors inherent in the printing process. This approach helps in evaluating the consistency of the printer and the reliability of the produced components under identical conditions.

2.1. Printing parameters

To generate the G-code for the test specimens, Prusa Slicer 2.6.1 [39] was employed, using preset settings for the Artillery Sidewinder X2 [40] and PLA [29] as the selected material. The following parameters were modified (Table 1):

The print bed was meticulously adjusted to ensure optimal precision, and the filament was dehumidified both before and during the printing process.

2.2. Scanning operations

All scans conducted with the Revopoint Mini followed a consistent procedure to avoid influencing scan results and subsequent comparisons. Optimal performance was achieved by keeping the scanner stationary and directed towards the rotating turntable. For each object position, a complete rotation was executed at a speed of 80 s/revolution. The frame acquisition speed was determined by the capabilities of the device (approximately 9 fps), resulting in approximately 720 frames for

Fig. 1. Methodology workflow.

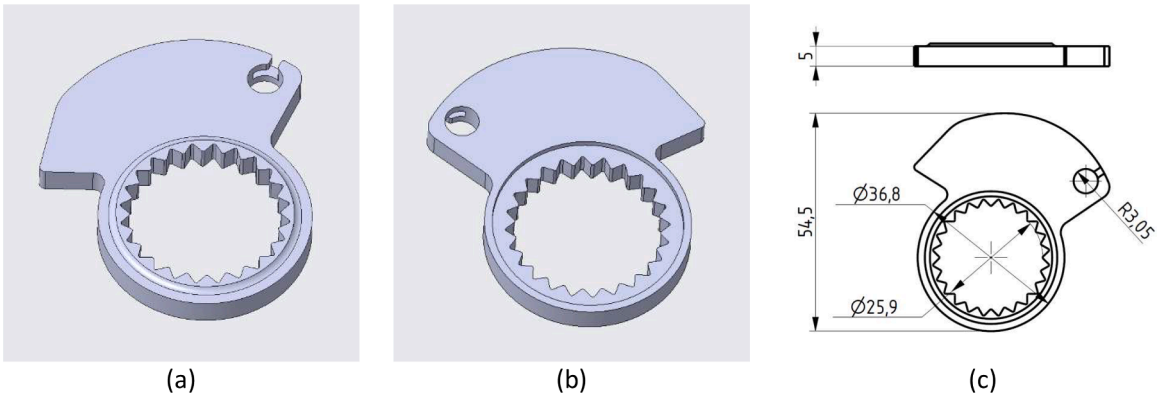

Fig. 2. Gas cam CAD model: (a) front view; (b) back view; (c) 2D drawing of the component with the most significant dimensions.

Table 1
3D printing parameters on Prusa Slicer.

Parameter	Value	Unit of mesure
Layer height / First layer height	0,1	mm
Solid layer: Top	5	/
Minimum shell thickness	0,5	mm
Thick bridges	No	/
Infill density	20	%
Infill pattern	Rectilinear	/
Maximum length of infill anchor	0	mm
Minimum skirt loops	0	mm
Default extrusion width	0,4	mm
First layer width	0,4	mm
Perimeters width	0,4	mm
External perimeter width	0,4	mm
Infill width	0,4	mm
Solid infill width	0,4	mm
Infill perimeter overlap	0	mm
G-code resolution	0,001	mm
Elephant foot compensation	0	mm
Enable support	Yes	/

each position to generate the point cloud.

The acquisition of the point cloud in 3D scanning depends on various factors. Some of these factors are controllable, such as the positioning of the object and the scanner, lighting conditions, contrast, and the calibration of the instrument. However, there are also non-controllable factors, primarily related to the scanner's software, which are managed by the scanner's processor and cannot be modified. These software parameters can significantly influence the quality of the point cloud, determining whether it is captured accurately or not.

Certain types of scanners may struggle with acquiring point clouds if the component has semi-transparent sections, specific colourations, or shiny or reflective surfaces. Specifically, the scanner used in this study performs well with white, green, and purple colours, while complementary colours are nearly invisible to the system. Given the choice, we selected a colour that the scanner detects best for this type of analysis. For components with difficult-to-detect surfaces or where changing the colour is not feasible, a special non-residual paint can be applied temporarily for the scanning process. This approach ensures that the filament colour does not affect the dimensional and geometric accuracy of the component.

In capturing the point cloud, it is crucial to avoid more than one complete rotation of the component, as this would result in re-scanning areas, leading to increased noise in the data. To mitigate manual handling vibrations, the scanner was mounted on a tripod. However, this static setup may cause certain areas to be less visible or have a lower point density. To address this limitation, six scanning positions were utilised, whereas typically, two or three positions are sufficient for a general acquisition. By carefully managing these factors, we aimed to optimise the scanning process to produce the most accurate and reliable point cloud representation of the components under study.

For each component, six scans were performed with six different orientations, as indicated in Fig. 3, to ensure comprehensive coverage of all sides of the component. Markers were used as reference points for capturing the point clouds, enhancing the precision of the point cloud for this type of component.

For the scan acquisition, the Revoscan software was used, allowing for the positioning of the object and the scanner in the correct orientation to generate the point cloud. As outlined in the workflow in Fig. 4, each point cloud was processed to reduce scan noise and cleaned of all markers before being exported from Revoscan. The decision was made to export the point clouds and merge them using Geomagic Design X [41], providing greater flexibility in the final mesh creation process.

Upon importing the point clouds into the environment, mesh generation is applied using the "General Mesh Generation" command. The algorithm involves predefined steps for point cloud alignment, mesh generation, and optimization. A conversion with a default workflow was chosen to avoid influencing the scan result.

2.3. Reliability

Before proceeding with the scanning of all 3D printed specimens, the reliability of the chosen scanner for this investigation was evaluated. This was done to assess the reliability and repeatability of scans using the Revopoint Mini, as the performance of such instruments can often vary from the data provided in the datasheet. The manufacturer declares a resolution of 0.02 mm and an accuracy of 0.05 mm.

The best choice would have been to use parallel blocks to assess the accuracy of the scanner, but the Revopoint scanner fails to capture a significant number of points due to the mirrored surface finish. Three independent complete scans of one of the specimens were performed with both the Revopoint and a high-end scanner (FARO Quantum S) known for its quality and precision in scanning, suitable for metrology and reverse engineering. The FARO Quantum S utilizes blue laser technology, coupled with an eight-axis arm that triangulates the probe's position for increased scanning precision.

The scans were compared, using the scan performed with the Faro as a reference, revealing an average error of 0.02 mm with a standard deviation following a Gaussian distribution. Therefore, it is possible to characterize the Revopoint scanner as reliable and with good repeatability for this specific application (Fig. 5).

2.4. Comparison method

The mesh derived from the CAD model serves as a reference, while the measured data comprises the meshes obtained from the scans. The comparison between the CAD model and the component scan was performed using Geomagic Control X, specifically developed for quality

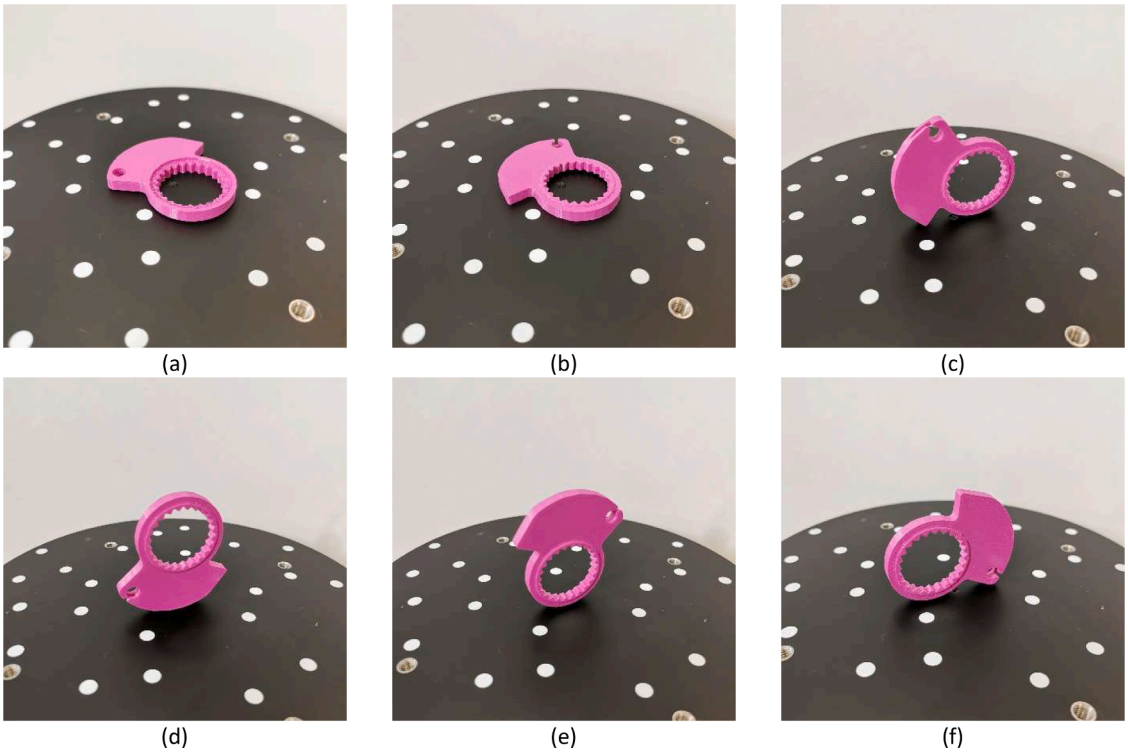

Fig. 3. Six cam positions on the rotary table that permit scanning: (a) one side of the cam; (b) the other side of the cam; (c) the small hole; (d) the cylindrical part; (e) the profile of the cam; (f) the flattener part of the cam. The dentation is captured partially in every scanning position.

Fig. 4. Workflow for scans performed with Revopoint.

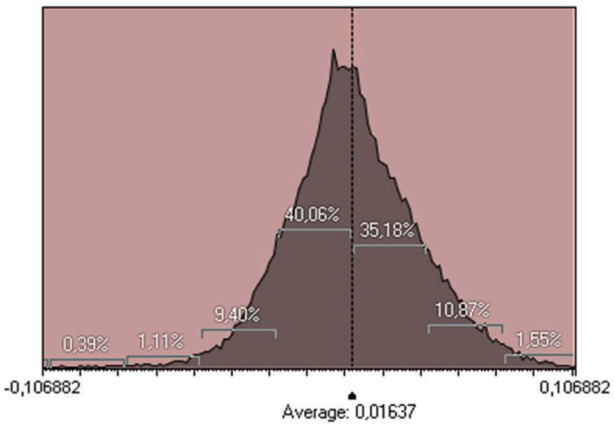

Fig. 5. The error in millimetres with Gaussian distribution in one of the comparisons between the scans performed with the two scanners.

control through these instruments. Prior to the comparison, it is necessary to align the CAD model and the scan using a best-fit alignment.

The comparisons conducted on each individual specimen include:

- "3D Compare": analysing the deviation between the reference and measured data by projecting all points normal to the reference surface. The deviation is depicted as a colour map, facilitating the analysis of positive and negative deviations in the component. The colour map's range can be customized based on specific requirements.
- "Silhouette Deviation": generates a silhouette from both the reference and the scan and analyses the deviation between them. This comparison is valuable for examining deviations in individual profiles in various projection directions.

The "3D Compare" command highlights areas with greater deviation through the generated colour map. To gain more detailed insights into individual components, the silhouette comparison was also employed, emphasizing areas more or less prone to error. The software does not permit the visualization or export of deviation values for individual points; access is limited to the mean value, root mean square (RMS), and standard deviation between reference and scanned component points.

The selected geometry features a small-sized cutout in a direction transverse to the printing direction. Since acquiring this feature with the scanner is challenging, the result may be approximated, leading to a peak error in that area (Fig. 6). As this is a small and isolated region, it does not significantly impact the analysed parameters but can be considered part of the scanning noise.

3. Result and discussion

The results obtained from the comparisons with the CAD model have yielded generally positive outcomes. Upon analysing the generated colour map, it becomes apparent that a significant portion of the model falls within the ±0.025 mm tolerance range. Other areas exhibiting deviations beyond the tolerance interval may either be positive,

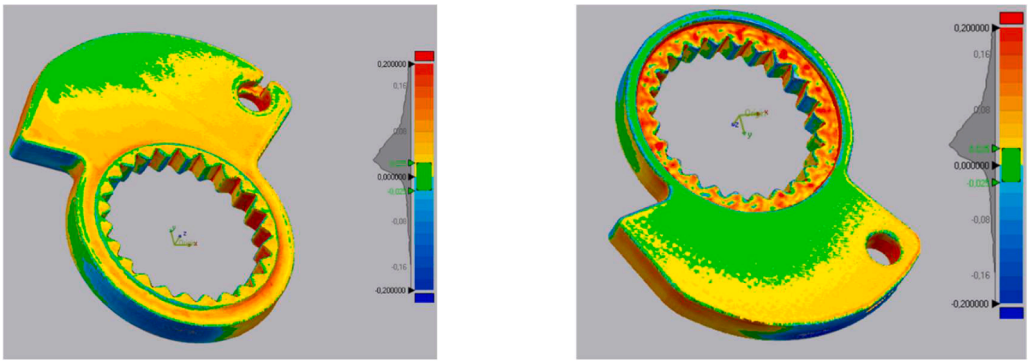

Fig. 6. "3D compare" applied to the gas cam: (a) front view; (b) back view.

meaning the point considered is outside the theoretical model, or negative. As depicted in Fig. 8, a colour scale ranging up to ±0.2 mm allows for differentiation of areas with greater deviation compared to others. The colour map is applied to the CAD model, facilitating rotation for assessing areas with geometric deformities. On the left side of the colour map legend, a graph indicates the distribution of all component points. This graph provides insights into the distribution of deviations based on value and the mode assumed by the value. Particularly for this component, it's evident that the majority of points are located outside the reference, as indicated by the peak of the graph being in the positive zone, and the area under the curve being greater in the positive interval than in the negative interval.

The areas exhibiting the greatest deformation, thus deviating the most from the original geometry, include the annular region of the cam, some teeth of the internal gear, and the mounting hole. The annular zone, visible in the intense red colour in the rear view, lacks a smooth surface finish due to the necessity of supports during the printing phase. The profile of the teeth appears imprecise due to their small size and intricate geometry; material deposition is not as accurate for small movements and sharp edges, such as the tooth tip. The hole exhibits a uniform red colour, indicating that it will be narrower because the actual surface has a uniform offset compared to the theoretical surface. Analysing the flat areas of the component in both views reveals slight deformation, likely attributable to thermal deformation during the component's cooling phase on the plane.

We can now shift our focus towards a more quantitative aspect of the analysis by scrutinizing the data obtained from mesh comparisons. Fig. 9 showcases a radar chart depicting the fundamental parameters utilized in this study, namely: alignment, 3D comparison, front silhouette, lateral silhouette, hole silhouette, and teeth silhouette. For each parameter, the mean value, root mean square, and standard deviation are provided for comprehensive examination.

Beginning with the assessment of mesh alignment, a commendable outcome is observed, as it demonstrates a mean error lower than the precision of the utilized scanner for measurements. While the 3D comparison offers a comprehensive evaluation of the component, its inclusion in the charts aims to ensure completeness, as its efficacy is predominantly conveyed through the colour map. The lateral silhouette showcases a minimal error falling within the margin of instrument error and alignment. Conversely, the frontal silhouette incorporates the profiles of the hole and dentition silhouettes, capturing information from three distinct perspectives (as depicted in Fig. 7a). Consequently, the profiles of the hole and dentition were isolated for analysis. The standard deviation of this parameter exhibits a marginally higher value compared to the preceding ones, indicating a greater dispersion of data. Nonetheless, it does not manifest a notable error relative to the diverse enclosed geometries.

In conclusion, it is evident that the last two parameters exhibit significantly higher errors compared to the preceding ones. The hole silhouette, in particular, features a markedly higher mean error than the other measured dimensions, albeit with a notably reduced standard deviation. This underscores the robust stability of the error within the hole. Since the error is positive, it results in a smaller hole compared to the mesh, yet with virtually consistent error distribution around the entire circumference. Conversely, the dentition silhouette presents a complex profile with a mean error exceeding a tenth of a millimetre. It is imperative to note that the standard deviation surpasses the error, indicating a high degree of fluctuation in the error within the dentition area.

Overall, the scanner offers significant flexibility in terms of scanning capabilities. It is a portable device that can be easily positioned within the workspace, and it comes at a much lower cost compared to equipment required for Computed Tomography (CT) or Scanning Electron Microscopy (SEM). The accuracy specified by the manufacturer has been

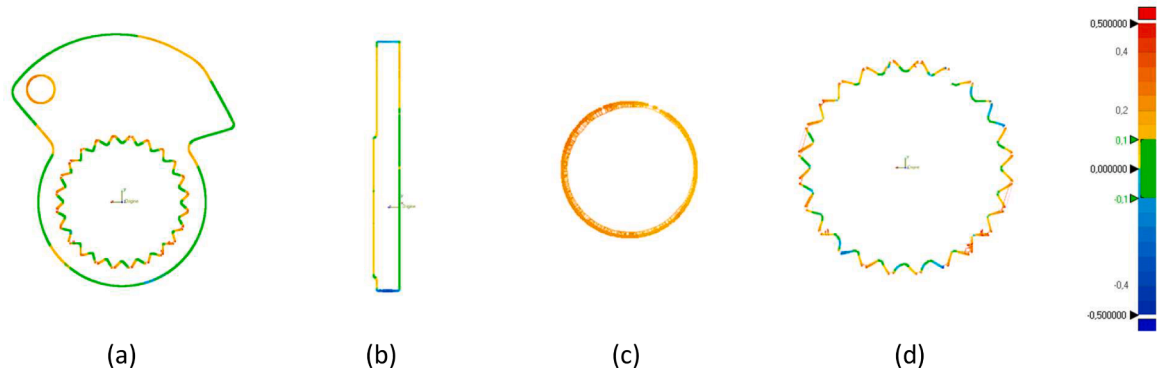

Fig. 7. Silhouette Deviation: (a) front, (b) lateral, (c) hole, (d) teeth. All images are created using the same colour scale, indicated on the right.

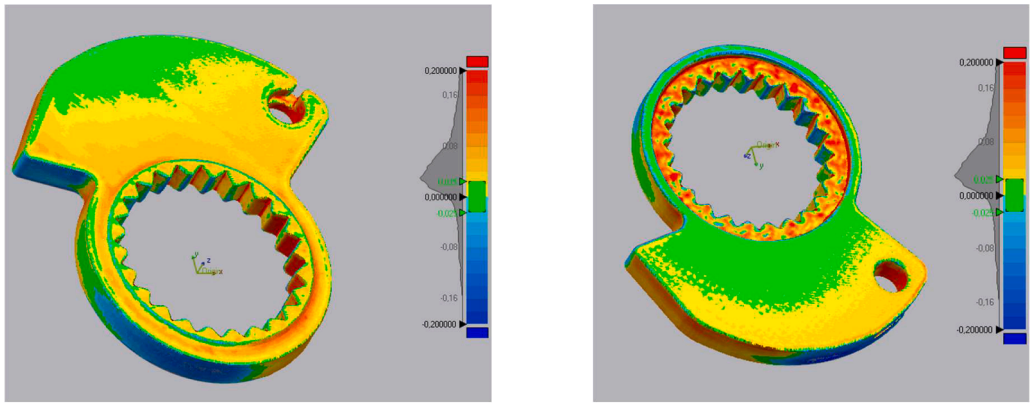

Fig. 8. Colour map of a gas cam: (a) front view; (b) back view.

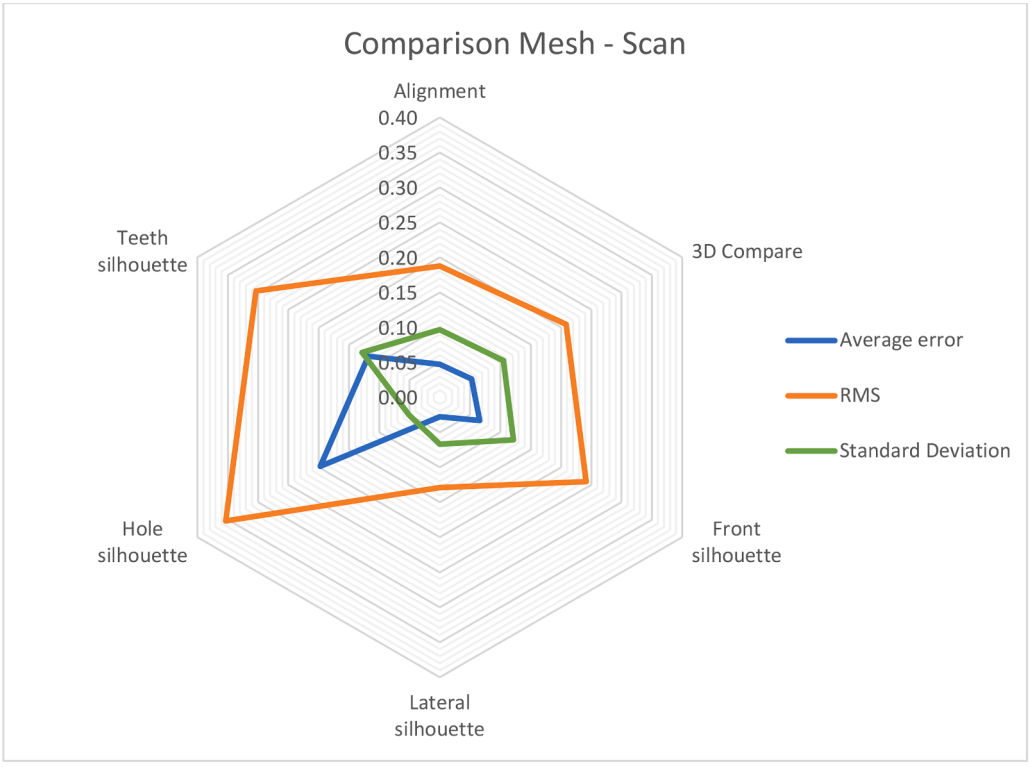

Fig. 9. Radar plot comparing mesh and scan data across six different parameters, considering the mean error, root mean square (RMS) error, and standard deviation (all values are in millimetres).

validated, allowing for precise and swift scans. However, there are inherent limitations; the scanner cannot analyse the internal structure of components, nor can it provide a sufficiently detailed view of the surface to measure surface roughness. Nevertheless, for assessing dimensional and geometric accuracy, this scanner proves to be a cost-effective tool compared to other technologies such as CT, SEM, or photogrammetry.

Each scanner operates within a defined scanning range, which is closely related to the precision of the resulting point cloud. This range restricts the scanner to capturing only a specific portion of space. If the object to be scanned falls within this range, it can be captured entirely in a single scan. For larger objects, it is necessary to scan the component in sections and then subsequently assemble the individual point clouds. The scanner we are employing has a field of view that can accommodate objects up to a maximum size of 200 × 200 × 200 mm. Despite this limitation, the process described above remains effective for larger objects by using multiple scans and merging the data.

Furthermore, samples with varying layer heights, specifically 0.10 mm, 0.15 mm, and 0.20 mm were also assessed to quantify the influence of layer height. No discernible variations in error were observed in relation to the parameters previously analysed in the radar chart. Nevertheless, through the colour map, discrepancies in error can be observed in features characterized by dimensions along the Z-axis that are not divisible by the layer height, such as the undercut of the dentition and the cavity on the external profile.

4. Conclusion

The study highlights the feasibility of employing a mid-to-low range 3D scanning device to produce models that are adequate for geometric and dimensional inspections. Such a device offers considerable

flexibility in analysing a variety of components, is easy to transport, and requires a relatively low financial investment.

However, it is important to note that surfaces or features exhibiting a process error of less than 0.05 mm cannot be accurately interpreted using this instrument due to its limited precision. The device proves effective in validating complex geometries, yet for small-scale details such as the component's gear teeth, it necessitates high-quality scanning to achieve a lower standard deviation.

Furthermore, it has been observed that the potential error introduced by varying layer height has an influence lower than the instrument's precision, rendering it unquantifiable through these analyses.

In summary, it is evident that quality control for components with complex geometries is achievable even with mid-to-low range instruments. However, careful attention must be paid to the type of feature under examination and the quality of the scan. For a more comprehensive verification process, it is recommended to utilize both the colour map to inspect critical areas of the component and the numerical results of the comparison to quantify errors.

CRediT authorship contribution statement

Andrea Montalti: Writing – original draft, Validation, Software, Resources, Methodology, Investigation, Formal analysis, Data curation, Conceptualization. **Patrich Ferretti:** Writing – original draft, Validation, Methodology, Formal analysis, Conceptualization. **Gian Maria Santi:** Writing – review & editing, Supervision, Project administration, Funding acquisition.

Declaration of competing interest

The authors declare that they have no known competing financial interests or personal relationships that could have appeared to influence the work reported in this paper.

Data availability

Data will be made available on request.

References

[1] N.D. Nguyen, I. Ashraf, W. Kim, Compact model for 3d printer energy estimation and practical energy-saving strategy, Electronics (Switzerland) 10 (4) (2021), https://doi.org/10.3390/electronics10040483.

[2] S. Fleury, B. Poussard, P. Blanchard, L. Dupont, P.M. Broekema, S. Richir, Innovative process for furniture design: contributions of 3D scan and virtual reality, Comput. Aided. Des. Appl. 19 (5) (2022), https://doi.org/10.14733/cadaps.2022.868-878.

[3] S.S. Crump, "US5121329A - apparatus and method for creating three-dimensional objects - google patents," 1989.

[4] N.A. Fountas, K. Kitsakis, K.E. Aslani, J.D. Kechagias, N.M. Vaxevanidis, An experimental investigation of surface roughness in 3D-printed PLA items using design of experiments, *Proc. Inst. Mech. Eng., Part J: J. Eng. Tribol.* 236 (10) (2022), https://doi.org/10.1177/13506501211059306.

[5] N. Vidakis, M. Petousis, E. Karapidakis, N. Mountakis, C. David, D. Sagris, Energy consumption versus strength in MEX 3D printing of polylactic acid, Adv. Ind. Manuf. Eng. 6 (2023), https://doi.org/10.1016/j.aime.2023.100119.

[6] N.A. Fountas, I. Papantoniou, J.D. Kechagias, D.E. Manolakos, N.M. Vaxevanidis, Modeling and optimization of flexural properties of FDM-processed PET-G specimens using RSM and GWO algorithm, Eng. Fail. Anal. 138 (2022), https://doi.org/10.1016/j.engfailanal.2022.106340.

[7] P. Żur, A. Kołodziej, A. Baier, G. Kokot, Optimization of Abs 3D-printing method and parameters, European J. Eng. Sci. Technol. 3 (1) (1970), https://doi.org/10.33422/ejest.v3i1.160.

[8] J. Wang, et al., Research of TPU materials for 3D printing aiming at non-pneumatic tires by FDM method, Polymers. (Basel) 12 (11) (2020), https://doi.org/10.3390/polym12112492.

[9] N. Vidakis, et al., Polyvinyl alcohol as a reduction agent in material extrusion additive manufacturing for the development of pharmaceutical-grade polypropylene/silver nanocomposites with antibacterial properties, Mater. Today Commun. 39 (2024) 109366, https://doi.org/10.1016/j.mtcomm.2024.109366. Jun.

[10] J. León-Becerra, M.Á. Hidalgo-Salazar, J.P. Correa-Aguirre, O.A. González-Estrada, A.D. Pertuz, Additive manufacturing of short carbon filled fiber nylon: effect of build orientation on surface roughness and viscoelastic behavior, Int. J. Adv. Manuf. Tech. 130 (1–2) (2024) 425–435, https://doi.org/10.1007/s00170-023-12503-w. Jan.

[11] S.J. Park, J.E. Lee, J. Park, N.K. Lee, Y. Son, S.H. Park, High-temperature 3D printing of polyetheretherketone products: perspective on industrial manufacturing applications of super engineering plastics, Mater. Des. 211 (2021), https://doi.org/10.1016/j.matdes.2021.110163.

[12] S. Qian, K. Bao, B. Zi, N. Wang, Kinematic calibration of a cable-driven parallel robot for 3D printing, Sensors (Switzerland) 18 (9) (2018), https://doi.org/10.3390/s18092898.

[13] S. Micalizzi, A.Díaz Lantada, C. De Maria, Shape-memory actuators manufactured by dual extrusion multimaterial 3d printing of conductive and non-conductive filaments, Smart. Mater. Struct. 28 (10) (2019), https://doi.org/10.1088/1361-665X/ab3b35.

[14] B. Regassa Hunde, A. Debebe Woldeyohannes, Future prospects of computer-aided design (CAD) – A review from the perspective of artificial intelligence (AI), extended reality, and 3D printing, Results. Eng. 14 (2022), https://doi.org/10.1016/j.rineng.2022.100478.

[15] A. Bacciaglia, A. Ceruti, A. Liverani, Photogrammetry and additive manufacturing based methodology for decentralized spare part production in automotive industry, Adv. Intell. Syst. Computing (2020), https://doi.org/10.1007/978-3-030-39512-4_121.

[16] A.D. Voicu, A. Hadăr, D. Vlăsceanu, Benefits of 3D printing technologies for aerospace lattice structures, Sci. Bull. Nav. Acad. 24 (1) (2021), https://doi.org/10.21279/1454-864X-21-I1-001.

[17] P. Ferretti, E. Fusari, G. Alessandri, M. Freddi, D. Francia, Stress-based lattice structure design for a motorbike application, F1000Res. 11 (2023) 1162, https://doi.org/10.12688/f1000research.125184.2. Nov.

[18] C. Parisot, M. Antonini, M. Barlaud, 3D scan-based wavelet transform and quality control for video coding, EURASIP. J. Appl. Signal. Processing. 2003 (1) (2003), https://doi.org/10.1155/S1110865703210064.

[19] N. Fountas, J. Kechagias, N. Vaxevanidis, Statistical modeling and optimization of surface roughness for PLA and PLA/Wood FDM fabricated items, J. Mater. Eng. 1 (1) (2023), https://doi.org/10.61552/jme.2023.01.005.

[20] J.D. Kechagias, K. Ninikas, M. Petousis, N. Vidakis, N. Vaxevanidis, An investigation of surface quality characteristics of 3D printed PLA plates cut by CO2 laser using experimental design, Mater. Manuf. Process. 36 (13) (2021), https://doi.org/10.1080/10426914.2021.1906892.

[21] J. Bernaczek, G. Budzik, T. Dziubek, Ł. Przeszłowski, K. Wójciak, Dimensional-shape verification of a selected part of machines manufactured by additive techniques, Adv. Sci. Technol. Res. J. 17 (1) (2023), https://doi.org/10.12913/22998624/157289.

[22] G. Jović, D. Ćirić, F. Pešić, M. Ivanović, M. Mijajlović, Deviation of the 3D solid model from the printed model, in: 2023 22nd International Symposium INFOTEH-JAHORINA, INFOTEH 2023, 2023, https://doi.org/10.1109/INFOTEH57020.2023.10094160.

[23] M. Wan, R. Zheng, S. Wang, H. Huang, H. Zhao, L. Yu, Efficient 3D scanning measurement system based on asymmetric trinocular vision and a multi-line laser, Appl. Opt. 62 (8) (2023), https://doi.org/10.1364/ao.481406.

[24] X. Ma, D. Wang, W. Li, X. Dai, S. Liu, Z. Li, Estimation of the skeletal muscle cross-sectional area of the lower extremity using structured light three-dimensional scanning technology, J. Med. Biol. Eng. 43 (4) (2023) 446–453, https://doi.org/10.1007/s40846-023-00816-w.

[25] S.-H. Baek, N. Walsh, I. Chugunov, Z. Shi, F. Heide, Centimeter-wave Free-space Neural Time-of-Flight Imaging, ACM Trans. Graph 42 (1) (2023), https://doi.org/10.1145/3522671.

[26] A.D.S.Á.B. de Oliveira, et al., Foundations and guidelines for high-quality three-dimensional models using photogrammetry: a technical note on the future of neuroanatomy education, Anat. Sci. Educ. 16 (5) (2023) 870–883, https://doi.org/10.1002/ase.2274.

[27] M. Colom, P. Ricci, M. Duocastella, Rapid quantification of 3D ultrasound fields with wavefront sensing and Schlieren tomography, Ultrasonics 135 (2023), https://doi.org/10.1016/j.ultras.2023.107115.

[28] G.W. Melenka, J.S. Schofield, M.R. Dawson, J.P. Carey, Evaluation of dimensional accuracy and material properties of the MakerBot 3D desktop printer, Rapid. Prototyp. J. 21 (5) (2015), https://doi.org/10.1108/RPJ-09-2013-0093.

[29] J.D. Kechagias, N. Vidakis, M. Petousis, N. Mountakis, A multi-parametric process evaluation of the mechanical response of PLA in FFF 3D printing, Mater. Manuf. Process. 38 (8) (2023), https://doi.org/10.1080/10426914.2022.2089895.

[30] J. Kechagias, S. Zaoutsos, Effects of 3D-printing processing parameters on FFF parts' porosity: outlook and trends, Mater. Manuf. Process. 39 (6) (2024), https://doi.org/10.1080/10426914.2024.2304843.

[31] N. Vidakis, C. David, M. Petousis, D. Sagris, N. Mountakis, A. Moutsopoulou, The effect of six key process control parameters on the surface roughness, dimensional accuracy, and porosity in material extrusion 3D printing of polylactic acid: prediction models and optimization supported by robust design analysis, Adv. Ind. Manuf. Eng. 5 (2022), https://doi.org/10.1016/j.aime.2022.100104.

[32] N. Vidakis, C. David, M. Petousis, D. Sagris, N. Mountakis, Optimization of key quality indicators in material extrusion 3D printing of acrylonitrile butadiene styrene: the impact of critical process control parameters on the surface roughness, dimensional accuracy, and porosity, Mater. Today Commun. 34 (2023), https://doi.org/10.1016/j.mtcomm.2022.105171.

[33] "https://global.revopoint3d.com/en-eur/products/industry-3d-scanner-min i".

[34] Y. Dessery, J. Pallari, Measurements agreement between low-cost and high-level handheld 3D scanners to scan the knee for designing a 3D printed knee brace, PLoS ONE 13 (1) (2018), https://doi.org/10.1371/journal.pone.0190585.
[35] A. Elayeb, A. Korbi, R. Bahloul, F. Zemzemi, M. Tlija, and B. Louhichi, "A CAD-based method for the measurement of AM parts accuracy considering the build orientation," 2024, pp. 107–113. doi: 10.1007/978-3-031-47784-3_14.
[36] R. Wichniarek, F. Górski, W. Kuczko, P. Zawadzki, P. Buń, Dimensional accuracy of parts manufactured by 3D printing for interaction in virtual reality, Adv. Sci. Technol. Res. J. 11 (4) (2017), https://doi.org/10.12913/22998624/80848.
[37] B.V. Chowdary, D. Jaglal, 3D CAD model reconstruction and fast prototyping of rotational parts: a reverse engineering approach, J. Eng. Des. Technol. 21 (5) (2023), https://doi.org/10.1108/JEDT-07-2021-0365.
[38] "https://help.prusa3d.com/it/category/prusaslicer_204".
[39] "https://www.artillery3d.com/products/artillery-sw-x2-fdm-3d-printer-larger-printed-size-300x300x400mm".
[40] "https://oqton.com/it/geomagic-designx/".
[41] "https://oqton.com/it/geomagic-controlx/".